AD NUMBER

AD290303

LIMITATION CHANGES

TO:

Approved for public release; distribution is unlimited.

FROM:

**Distribution authorized to U.S. Gov't. agencies and their contractors;
Administrative/Operational Use; NOV 1962. Other requests shall be referred to Air Force Arnold Engineering Develoment Center, Arnold AFB, TN.**

AUTHORITY

aedc ltr, 12 dec 1975

AEDC-TDR-62-195

PRESSURES AND FORCES ON A MISSILE MODEL RESULTING FROM STAGE SEPARATION AT VERY HIGH ALTITUDES

By

T. W. Binion, Jr. and R. D. Herron

Propulsion Wind Tunnel Facility
ARO, Inc.

TECHNICAL DOCUMENTARY REPORT NO. AEDC-TDR-62-195

November 1962

AFSC Program Area 750A, Project 8953, Task 895301

(Prepared under Contract No. AF 40(600)-1000 by ARO, Inc., contract operator of AEDC, Arnold Air Force Station, Tenn.)

ARNOLD ENGINEERING DEVELOPMENT CENTER

AIR FORCE SYSTEMS COMMAND

UNITED STATES AIR FORCE

PRESSURES AND FORCES ON A MISSILE MODEL RESULTING FROM STAGE SEPARATION AT VERY HIGH ALTITUDES

By

T. W. Binion, Jr. and R. D. Herron

Propulsion Wind Tunnel Facility

ARO, Inc.

a subsidiary of Sverdrup and Parcel, Inc.

November 1962

ARO Project No. 200112

AF - AEDC
Arnold AF Stn Tenn

ABSTRACT

Pressure and force measurements were obtained on models of two missile stages during stage separation. The upper stage rocket engine exhaust was simulated with high pressure carbon dioxide. Data were obtained at seven separation distances with an upper stage nozzle exit pressure ratio variation from 52 to 8,066. The test cell pressure ranged from 1.25 to 750 microns of mercury which corresponds to an altitude range from 290,000 to 160,000 ft.

The results indicate that the pressures and forces on the lower stage are independent of ambient pressure and are dependent on engine chamber pressure and stage separation distance. At separation distances less than two engine nozzle diameters, the lower stage will affect the pressures and forces on the upper stage.

PUBLICATION REVIEW

This report has been reviewed and publication is approved.

A. Lincoln Coapman
Major, USAF
Acting AF Representative, PWT
DCS/Test

Jean A. Jack
Colonel, USAF
DCS/Test

CONTENTS

TABLE

ILLUSTRATIONS

NOMENCLATURE

A	Upper stage cross-sectional area, 3.546 in.^{2}
D	Lower stage drag, lb, positive acting downstream
d	Upper stage nozzle exit diameter, 1.25 in.
F_a	Upper stage thrust, lb, positive acting upstream
H_c	Upper stage engine chamber pressure, psi
p	Local static pressure, psi
p_e	Upper stage nozzle exit static pressure, microns of mercury
p_g	Lower stage tank dome static pressure, psi (see Fig. 4b)
p_∞	Altitude pressure, microns of mercury
R	Upper stage model radius, 1.0625 in.
r	Radius, in.
x	Distance between upper stage base and the leading edge of interstage fairing (see Fig. 4a)

1.0 INTRODUCTION

One of the critical operations during a missile flight concerns stage separation. If the upper stage ignition occurs too soon after separation, interference with the lower stage can adversely affect the operation and performance of the upper stage. A long interval between stage separation and upper stage ignition results in an extended coast time, which could also adversely affect missile performance. A knowledge of the forces, pressures, and flow field about the two stages during separation could lead to an optimum coast time for the staging operation.

The investigation reported herein was undertaken to determine the effect of the upper stage exhaust on the pressures and forces about the two stages during separation. The tests were conducted under the sponsorship of the Arnold Engineering Development Center (AEDC), Air Force Systems Command (AFSC), in the Cold Wall Vacuum Chamber. The tests were conducted utilizing carbon dioxide as the upper stage propellant. The altitude pressure in the test chamber was a function of several operating parameters and, therefore, was a dependent variable. However, an effective altitude variation was accomplished through the parameter nozzle exit pressure/test cell pressure. Data were obtained at seven stage separation distances x/d from 1.04 to 9.04, with a rocket chamber pressure variation of 6 to 100 psi, which resulted in an exit pressure ratio variation from 52 to 8,066.

2.0 APPARATUS

2.1 TEST CHAMBER

The Cold Wall Vacuum Chamber was designed to allow testing at altitudes in the 200,000-ft range with cold surfaces being utilized to cryopump a simulated rocket exhaust. Carbon dioxide was selected as the rocket exhaust because it can be readily cryopumped at liquid nitrogen temperatures. The CO_2 must be superheated to about 500°F to prevent the gas from condensing in the test region as it expands to the altitude pressure.

The Cold Wall Vacuum Chamber complex, shown in Fig. 1, consists of four systems: the vacuum chamber, mechanical pumps, liquid nitrogen supply, and carbon dioxide supply. The vacuum chamber, shown in

Manuscript released by authors September 1962.

Fig. 2, is a right circular cylinder, 36 inches in diameter and 158 inches long. The vacuum chamber wall is constructed from double wall panels through which liquid nitrogen is circulated. Approximately 110 ft^2 of the surface area can be cooled to -320°F to cryopump the simulated rocket exhaust. The chamber is equipped with two model support structures and a 16-inch-diameter area for model observation and flow visualization between the supports. The vacuum chamber installation is shown in Fig. 3.

The mechanical pumping system consists of two 15-hp rotary pumps with a total pumping speed of 500 cfm. Liquid nitrogen is supplied from a pump-equipped transport trailer. Liquid nitrogen can be delivered at rates from zero to 250 gpm.

The carbon dioxide system consists of a portable liquid storage unit, a pump, and a conditioning vessel. The CO_2 is introduced into the 60-ft^3 conditioning vessel as a liquid at 300 psi and 0°F. It is then superheated to 500°F by 70 one-kilowatt heater units, with the resulting pressure dependent upon the mass of CO_2 in the vessel. However, the maximum pressure allowable in the conditioning vessel is 1,350 psi.

2.2 MODELS

The basic dimensions of the models and the pressure orifice locations are presented in Fig. 4. The upper stage nozzle has an area ratio of 8.33. The gas properties at the nozzle exit were calculated by assuming a thermodynamic equilibrium isentropic expansion from stagnation conditions. The stagnation temperature was taken as 500°F. The nozzle exit conditions thus obtained are: Mach number, 3.25; static pressure/total pressure ratio, 0.013; static temperature, -76°F; and specific heat ratio, 1.34.

The lower stage tank dome is a spherical segment with a radius equal to the interstage inside diameter. The thickness of the interstage fairing could not be scaled because of strength requirements; however, the outer surface of the fairing was tapered to reduce its thickness as much as possible. The axial position of the lower stage was adjusted by manually positioning the sting in its support.

2.3 INSTRUMENTATION

Model instrumentation consisted of 12 pressure orifices on the lower stage model and five on the upper stage model, as shown in Fig. 4,

plus the upper stage chamber pressure orifice. The 18 model pressures were measured by Precision Pressure Balance transducers. The lower stage forces were measured with a three-component internal balance, and the upper stage axial force was measured by strain gages located on the carbon dioxide supply piping, as indicated in Fig. 4a.

The vacuum chamber instrumentation consisted of two pressure orifices, one in each end of the test cell. The cell pressure in the model end of the cell was measured by a Pirani gage, while the downstream pressure was measured with an Alphatron gage. Nineteen thermocouples were used to measure gas and structure temperatures in the cell.

3.0 PROCEDURE

The day prior to testing, the CO_2 conditioning vessel was filled with approximately 300 lb of carbon dioxide, and superheating was begun. Approximately six hours were required to heat the CO_2 to 500°F. A thermostat control device was then employed to maintain the temperature at 500°F. Pumpdown of the vacuum chamber required about ten minutes; however, the chamber was kept in an evacuated condition whenever possible.

Chilldown of the vacuum chamber was begun when the cell pressure reached the minimum pressure attainable with the mechanical pumps. It was discovered that chilldown should proceed slowly to allow a good frost coat to form on the outside of the cell. If chilldown proceeded too quickly, the outside walls would become cold enough to condense air, and a mixture of liquid air and frost would result. Consequently, chilldown required about one hour. However, because of the superior insulating properties of the frost over the liquid air-frost mixture, about 50 percent less liquid nitrogen was required for the slower method.

Upon completion of chilldown and immediately prior to firing the CO_2 rocket, the nitrogen flow was increased. The "firing" was accomplished by opening the two shutoff valves (Fig. 1) and manually loading the pneumatic throttling valve. Data recording was begun as soon as chamber pressure became stable at the desired value. The average "firing" time was 1.5 minutes. The "firing" was terminated by closing the throttle valve. Data were obtained at an average of seven chamber pressure settings at each separation distance. The cell was then allowed to warm so the condensed CO_2 could sublimate and be pumped out of the cell before the axial position of the model was adjusted.

4.0 RESULTS AND DISCUSSION

Data were obtained at seven stage separation distances, $x/d = 1.04$ to 9.04, with a chamber pressure varying from 6 to 100 psi. At stage separation distances less than $x/d = 4$, the pressure in the upstream portion of the cell, p_∞, rose during each firing to a stable value which was a function of rocket chamber pressure, separation distance and liquid nitrogen flow rate. The pressure rise was caused by reverse flow of CO_2 which could not be condensed because of insufficient cooling capacity in the upstream portion of the cell. A summary of test conditions presented in Table 1 shows that test cell pressure varied from 1.25 to 750 microns of mercury, which corresponds to an altitude variation from 290,000 to 160,000 ft.

The effect of nozzle exit pressure ratio, p_e/p_∞, which is an altitude effect, on the tank dome pressure ratio is presented in Fig. 5. The variation in p_e/p_∞ was limited at the lower separation distances because of the reverse flow discussed above. However, the data at x/d greater than two indicate that the tank dome pressure ratio is independent of p_e/p_∞. Therefore, if the rocket chamber pressure is constant, the tank dome pressure ratio is independent of the altitude at which separation occurs. The apparent scatter in the tank dome pressure ratio at x/d less than two may be caused by a shock system, within the interstage cavity, which is sensitive to engine chamber pressure. However, the variation of tank dome pressure ratio with separation distance (Fig. 6) indicates a very rapid change of the pressure ratio at low separation distances, and therefore some scatter in the data of Fig. 5 is to be expected.

It may be seen from Fig. 6 that the tank dome pressure ratio is dependent primarily on separation distance. Further, it is apparent that the absolute value of the tank dome pressure, p_9, is directly proportional to the chamber pressure, H_c, since p_9/H_c may be considered single-valued at each separation distance. As indicated in Fig. 5, p_9/H_c is independent of altitude. The altitude independence is a result of the relatively high energy level of the exhaust gases overshadowing any altitude effect which may be present. The jet pressures are on the order of 10^5 to 10^6 larger in magnitude than the altitude pressure. The lower stage, therefore, is sensitive only to the flow field of the jet and is not directly affected by the surroundings.

The static pressure distributions on the lower stage tank dome and interstage fairing for various chamber pressures at $x/d = 4.04$, 1.54, and 1.04 are presented in Fig. 7. The pressures on the external surface were less than the transducer sensitivity, i.e., 0.001 psi. At large

separation distances, a normal shock is present in front of the lower stage, and the fluid within the interstage cavity is stagnant. The lower stage acts as a large pitot tube, and the pressure within the cavity will be practically uniform, as shown at x/d = 4.04 in Fig. 7a. The pressure distribution at x/d = 4.04 is typical of all separation distances greater than x/d = 1.54. When the nozzle exit is within the interstage cavity, x/d = 1.04, the nozzle flow must turn 180 deg and escape through the annulus between the interstage fairing and the nozzle. The resulting pressure distribution within the cavity at x/d = 1.04 is shown in Fig. 7c. The pressure distribution at an intermediate position, x/d = 1.54, is shown in Fig. 7b. The pressure distributions shown by orifices 1 through 6 indicate a velocity gradient in the interstage cavity at the higher chamber pressures. Because of geometrical considerations, the velocity in this region must be toward the upper stage. Apparently, the high pressure core of the jet has penetrated into the cavity resulting in a 180-deg velocity change for at least a portion of the jet mass flow. A comparison of orifices 1 through 6 at x/d = 1.04 and 1.54 indicates that the velocity in the annulus is much higher at x/d = 1.04, as would be expected.

The upper stage base static pressure distribution for x/d = 1.54 and 1.04 is presented in Fig. 8. Base pressure on the upper stage was less than 0.001 psi at stage separation distances greater than x/d = 1.54. It is evident that a part of the nozzle flow had been turned back at x/d = 1.54, and there is relatively strong impingement at x/d = 1.04.

The strength of the flow impingement on the upper stage at x/d = 1.04 and 1.54 is clearly indicated by the thrust measurement shown in Fig. 9. Even though the pressure measured on the lower stage at x/d = 1.04 (Fig. 7c) is greater than the theoretical nozzle exit pressure (0.013 H_c), the flow within the nozzle is apparently fully developed, since substracting the force caused by the base pressure brings the measurements into agreement with the data at other positions where no interference was indicated.

It can be seen in Fig. 10 that the force on the lower stage is directly proportional to the upper stage chamber pressure at each separation distance. This fact is also implied in Fig. 6 wherein dividing the tank dome pressure by the chamber pressure reduces the data to a single curve. The normalized force data for both stages are presented in Fig. 11. The additional upper stage thrust, which is caused by interference with the lower stage, at x/d less than two is clearly evident. As the separation distance approaches zero, the parameters F_a/H_cA and D/H_cA increase rapidly and should approach unity.

5.0 CONCLUSIONS

Pressures and forces were obtained on two simulated missile stages at separation distances, x/d, from 1.04 to 9.04 and nozzle exit static pressure ratios, p_e/p_∞, from 52 to 8,066. The results indicate the following conclusions:

1. The pressures and forces on the upper stage are affected by the presence of the lower stage at x/d less than two.
2. The flow within the upper stage nozzle is not significantly affected at separation distances as close as x/d = 1.04.
3. The pressures and forces on the lower stage are independent of the ambient pressure.
4. The pressures and forces on the lower stage are dependent upon engine chamber pressure and separation distance.

TABLE I

SUMMARY OF TEST CONDITIONS

x/d	H_c, psi	p_∞, μ of Hg	p_e/p_∞	x/d	H_c, psi	p_∞, μ of Hg	p_e/p_∞
9.04	7.5	4.5	1120	2.04	10.0	80	84.0
	10.0	1.25	5376		15.0	150	89.6
	15.0	1.4	7196		20.0	75	134.0
	30.0	2.5	8066		30.0	175	115.0
	50.0	155.0	217		50.0	450	74.6
	67.0	6.0	7508		67.0	500	90.0
	100.0	175.0	384				
5.04	15.0	3.7	2725	1.54	10.0	50	134.0
	20.0	5.0	2689		14.5	130	74.8
	50.0	10.0	3361		19.5	170	77.3
	50.0	23.7	1418		30.0	250	80.6
	50.0	45.0	747		50.0	450	74.7
	67.0	155.0	290		67.0	450	100.0
	67.5	32.0	1418		67.0	700	64.3
4.04	10.0	8.5	791	1.04	9.0	115	52.6
	20.0	15.5	867		20.0	230	58.4
	20.0	19.3	696		30.0	300	67.2
	30.0	40.0	504		50.0	500	67.2
	50.0	75.0	448		67.0	500	90.0
	67.0	90.0	500				
	100.0	750.0	89.6				
3.04	6.0	20.7	195				
	15.0	19.0	528				
	20.0	32.0	420				
	30.0	80.0	252				
	50.0	140.0	240				
	50.0	170.0	198				
	67.0	300.0	150				

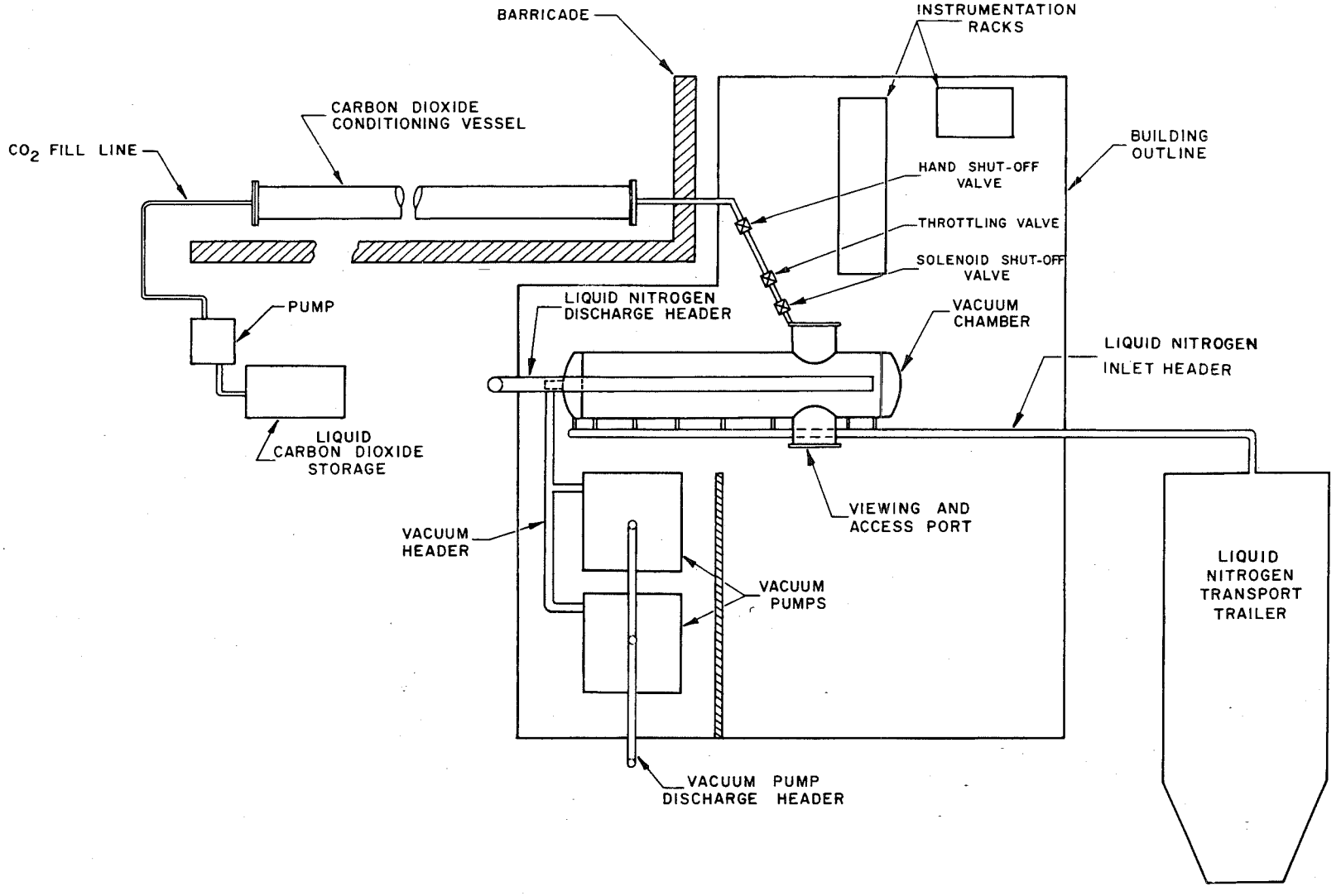

Fig. 1 Cold Wall Vacuum Chamber Complex

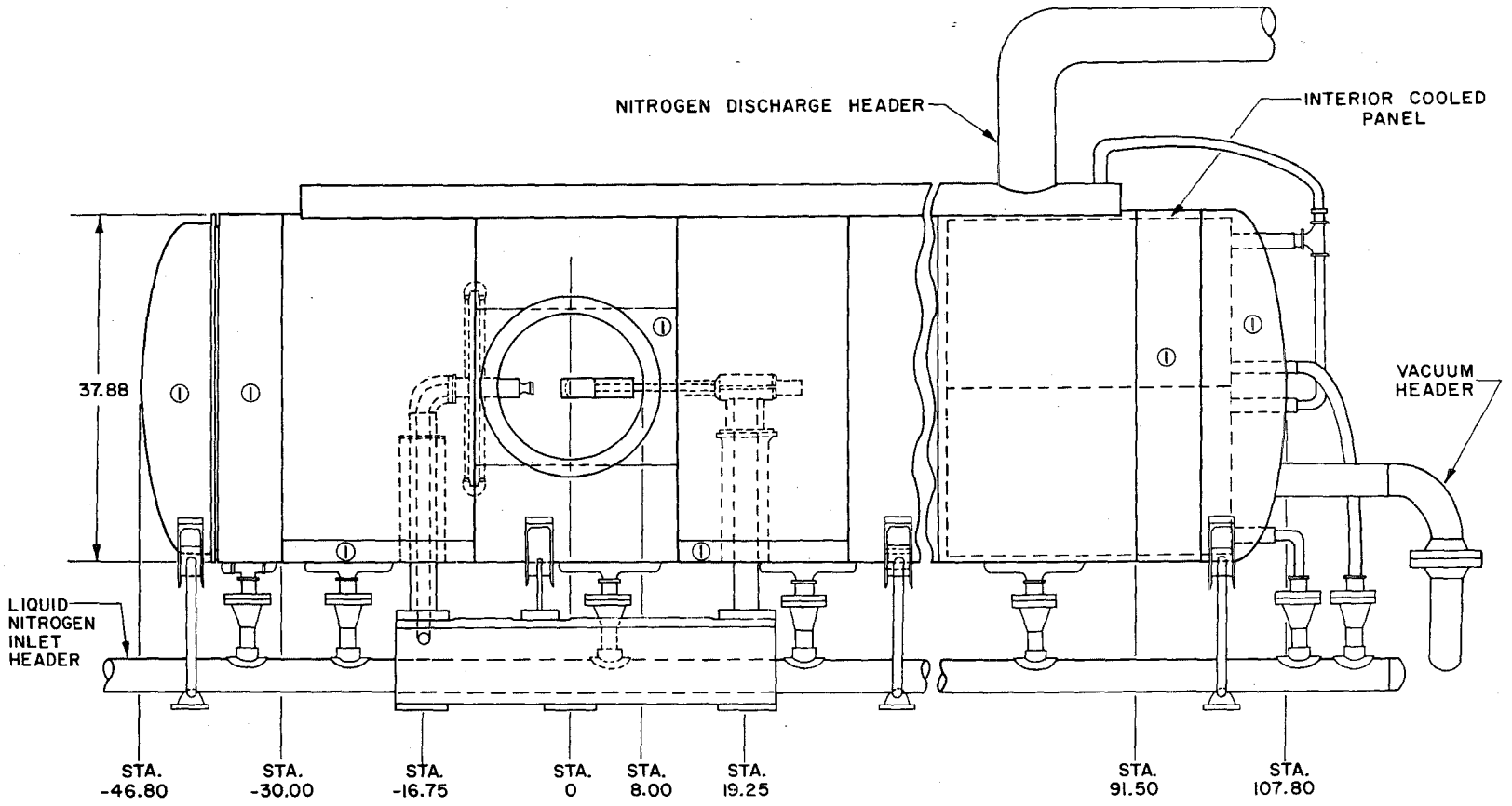

Fig. 2 Cold Wall Vacuum Chamber

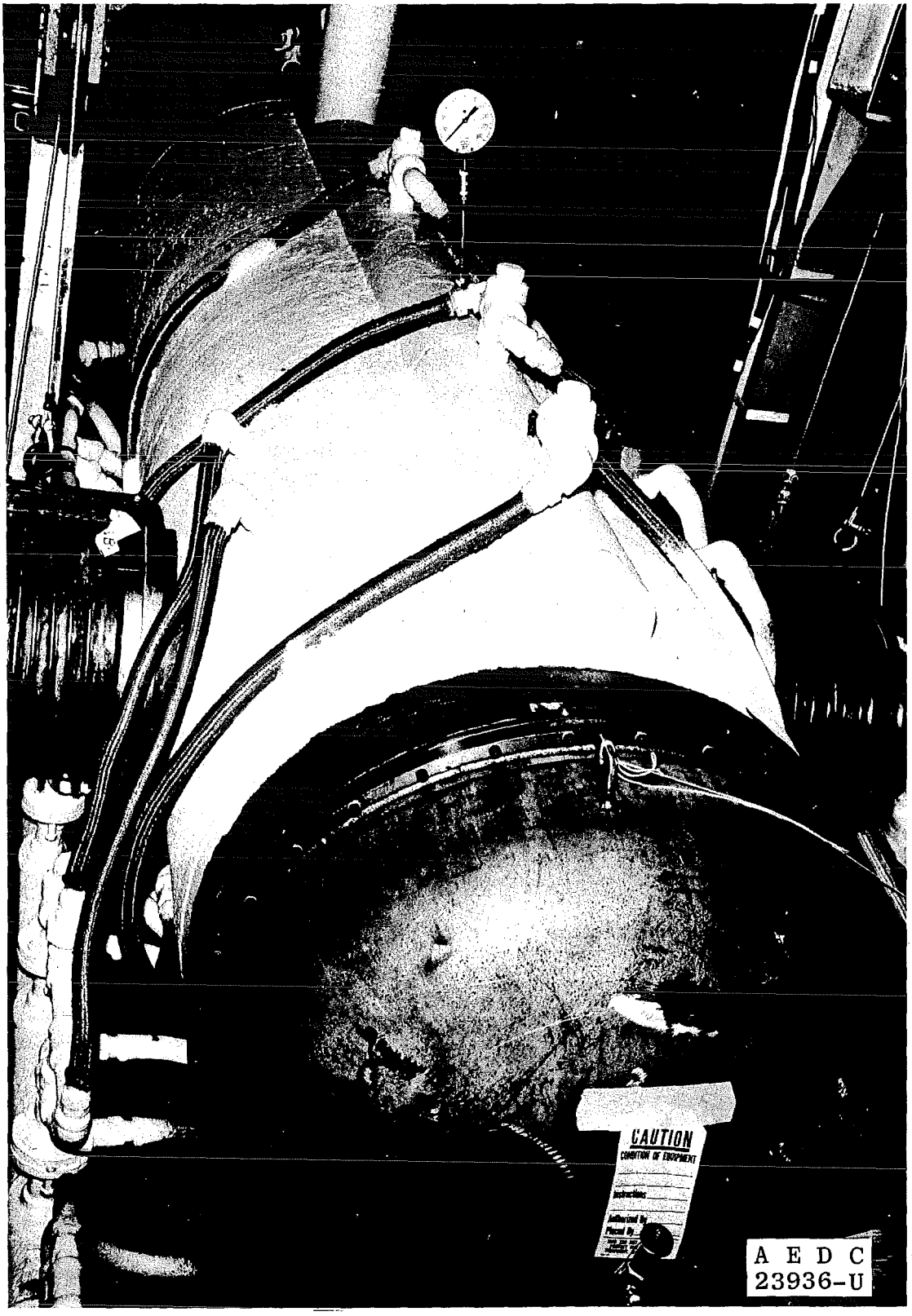

a. Top Three-Quarter View

Fig. 3 Vacuum Chamber Installation

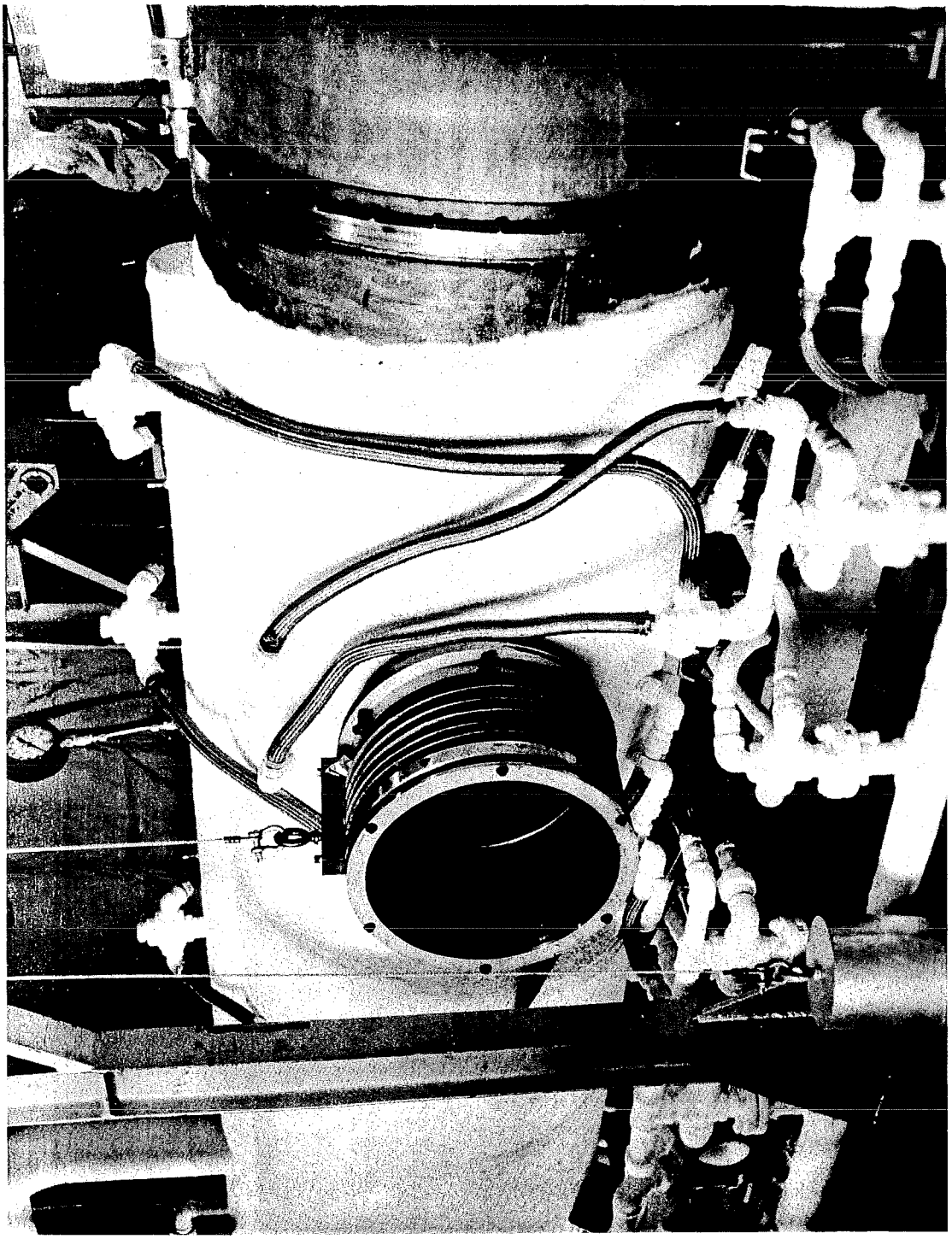

b. Side Three-Quarter View

Fig. 3 Concluded

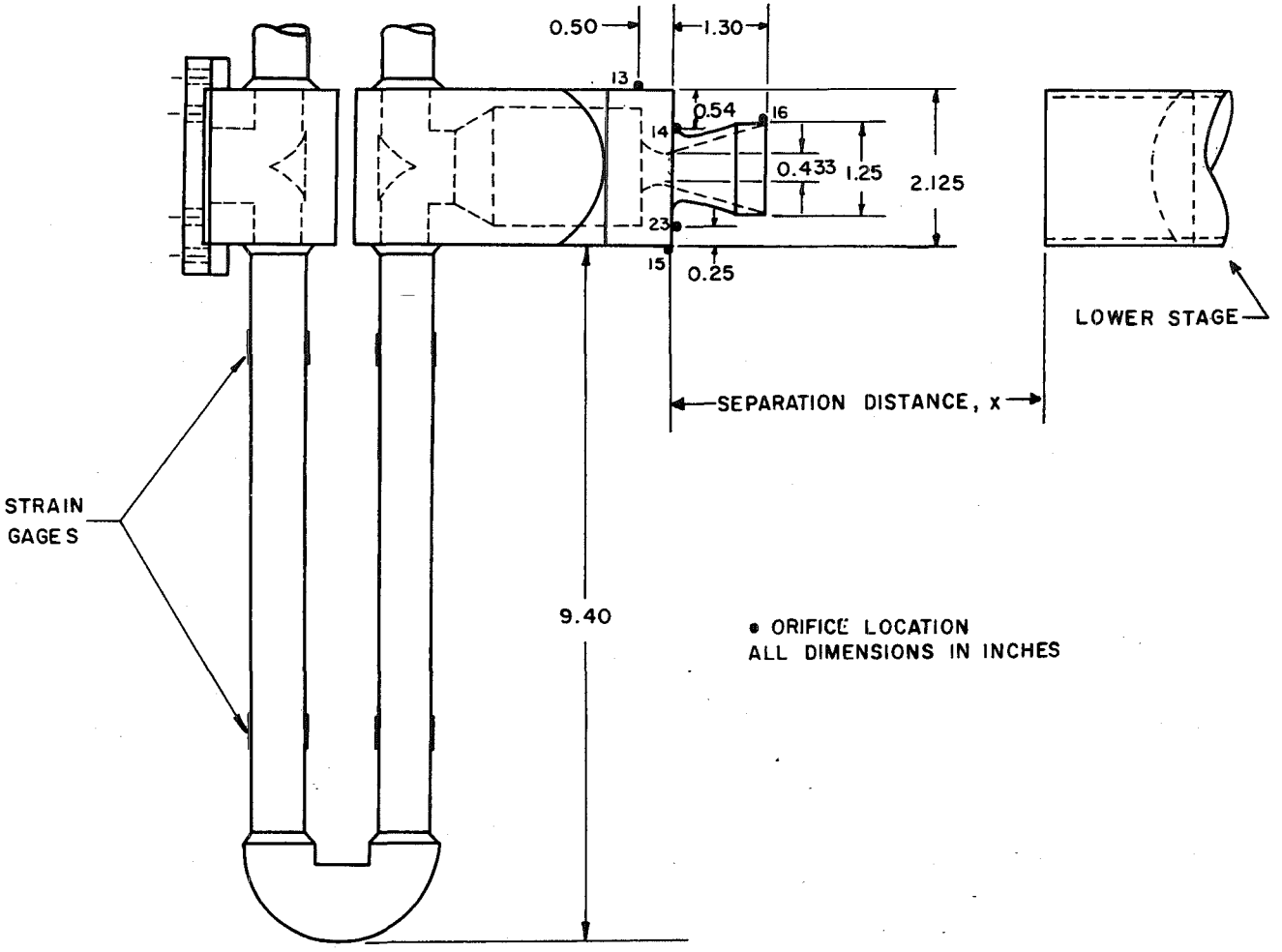

a. Upper Stage

Fig. 4 Model Configurations

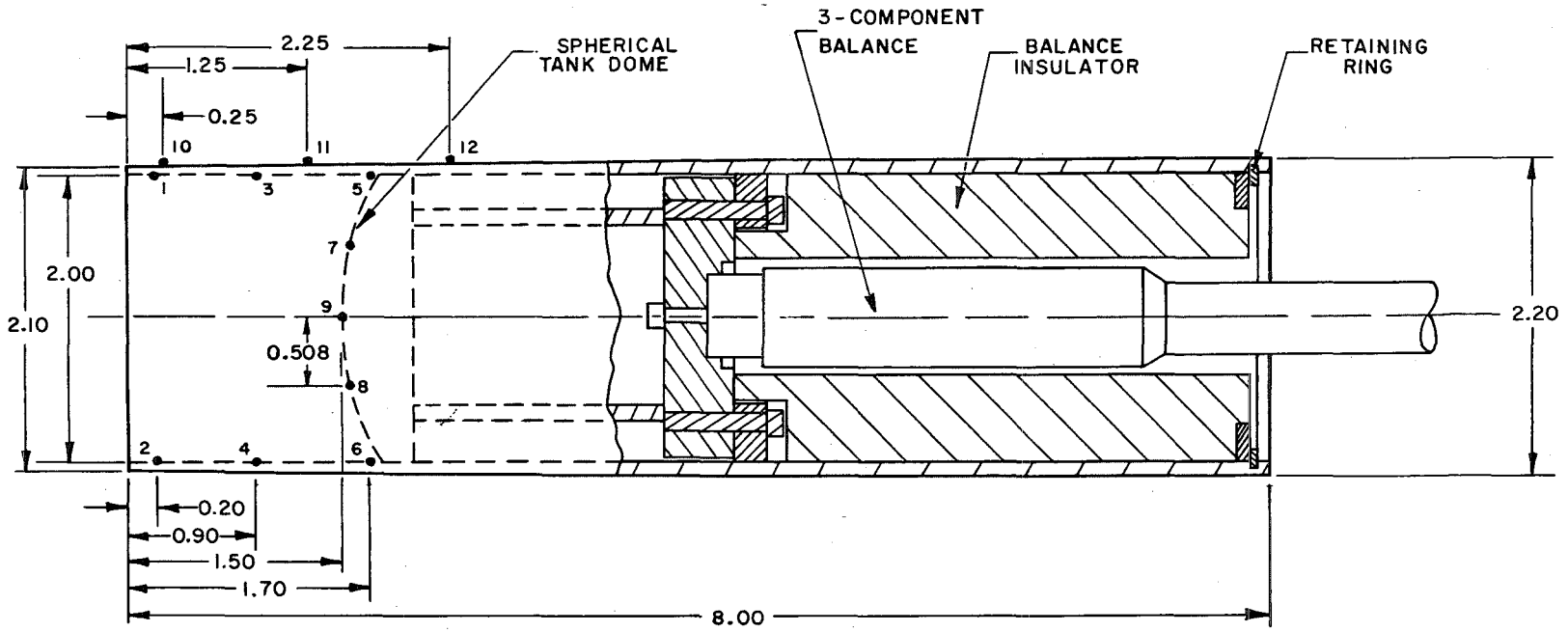

● ORIFICE LOCATION
ALL DIMENSIONS IN INCHES

b. Lower Stage

Fig. 4 Concluded

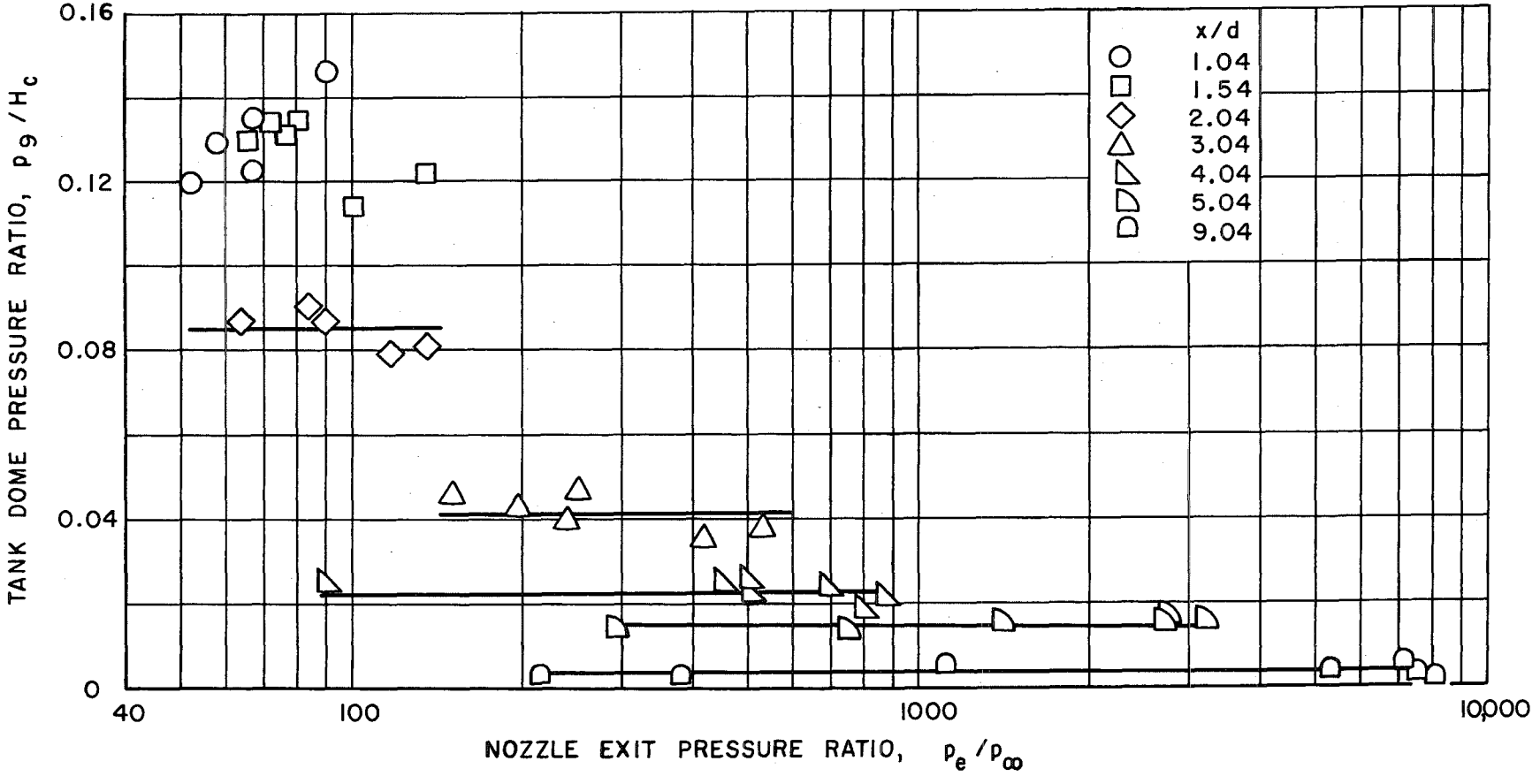

Fig. 5 Effect of Nozzle Exit Pressure Ratio on Tank Dome Pressure Ratio

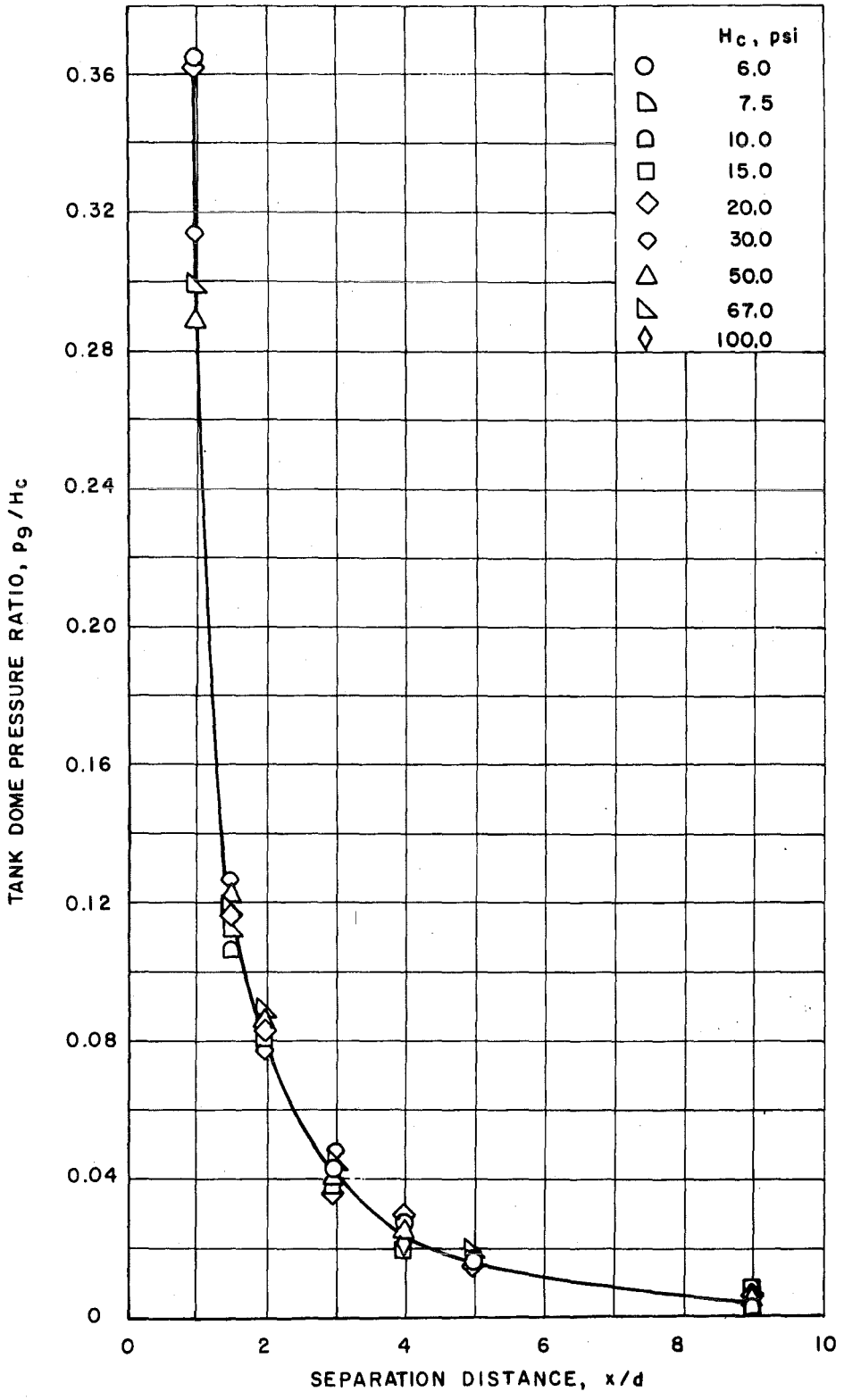

Fig. 6 The Effect of Separation Distance on Tank Dome Pressure Ratio

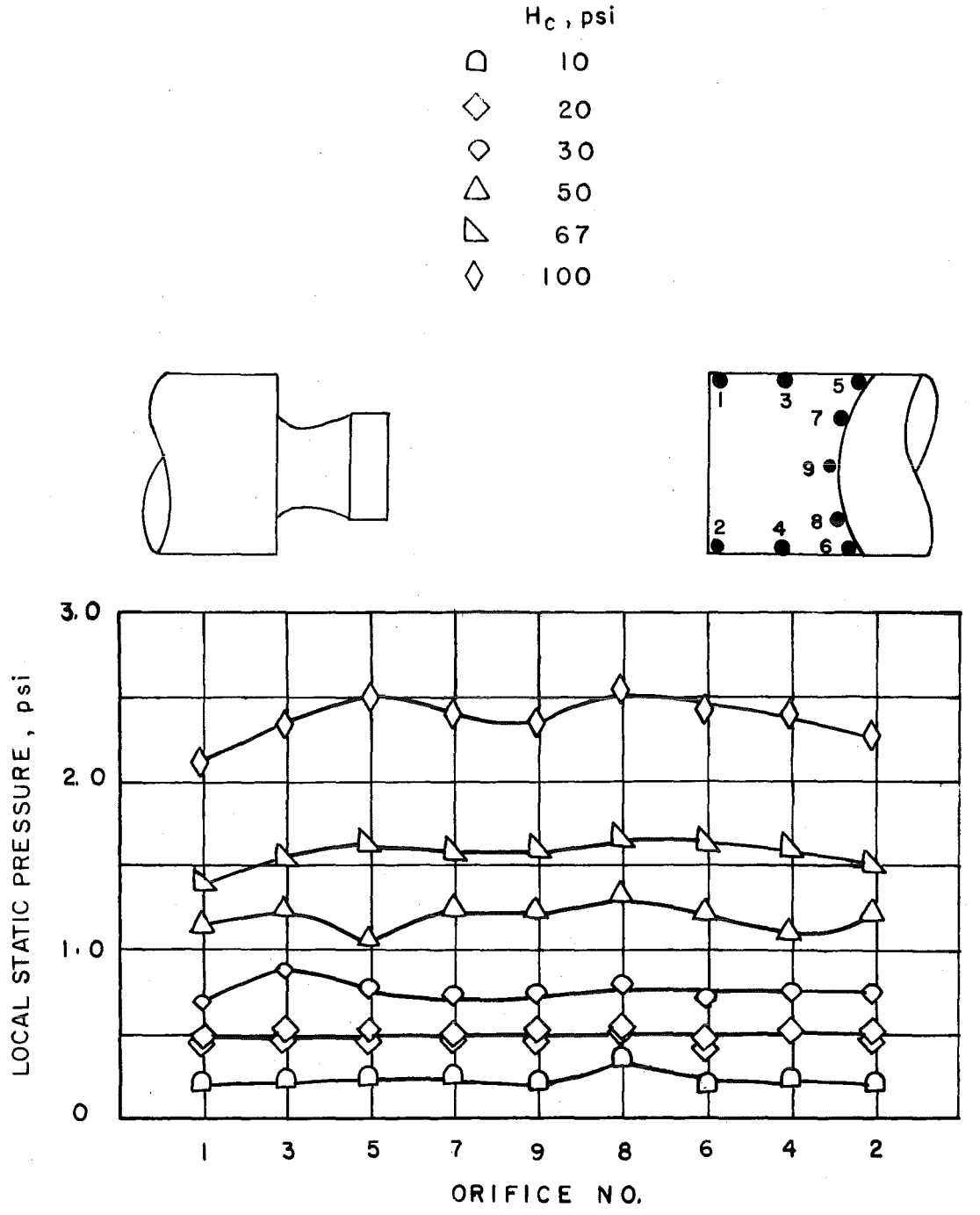

a. x/d = 4.04

Fig. 7 Lower Stage Static Pressure Distribution

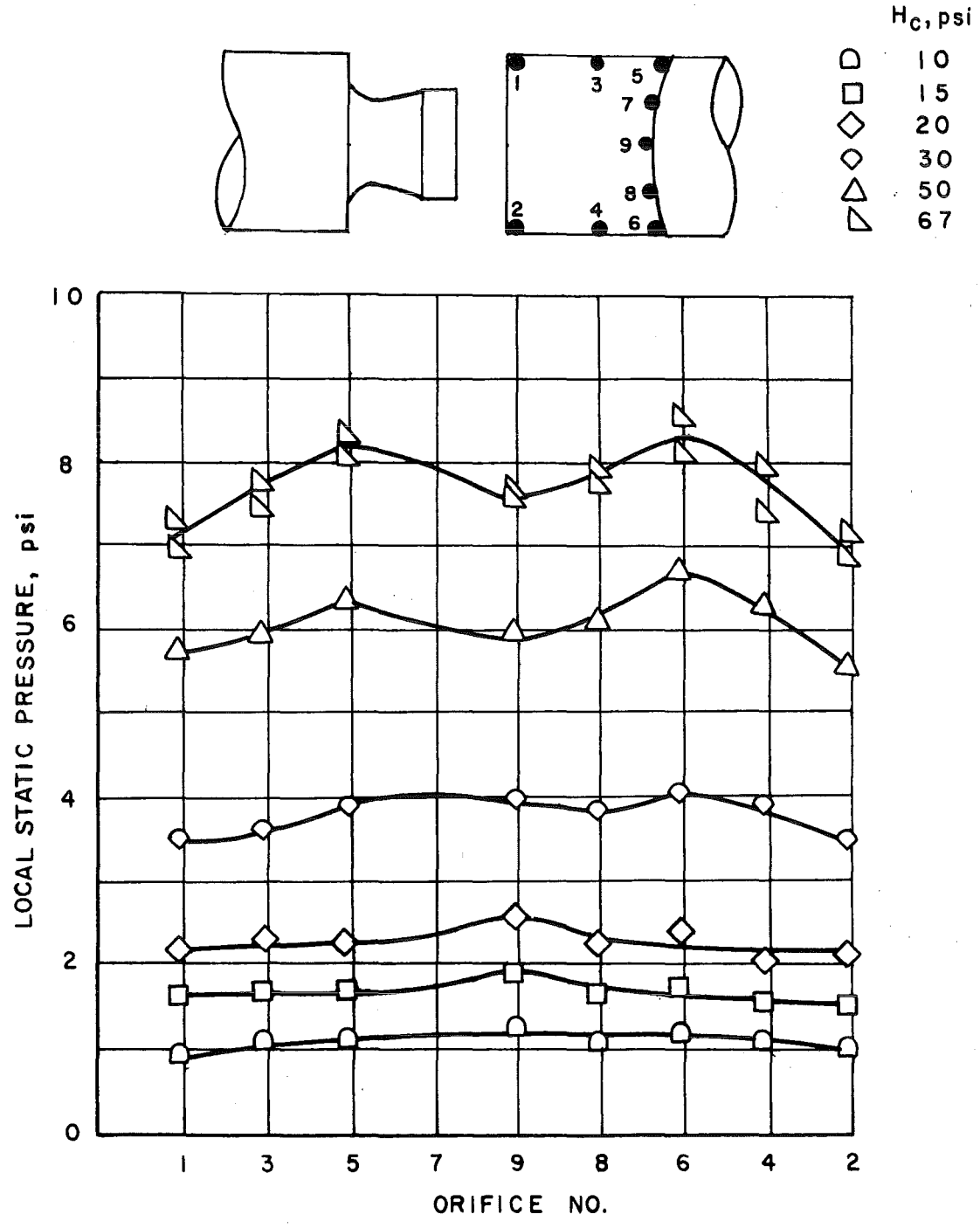

b. x/d = 1.54

Fig. 7 Continued

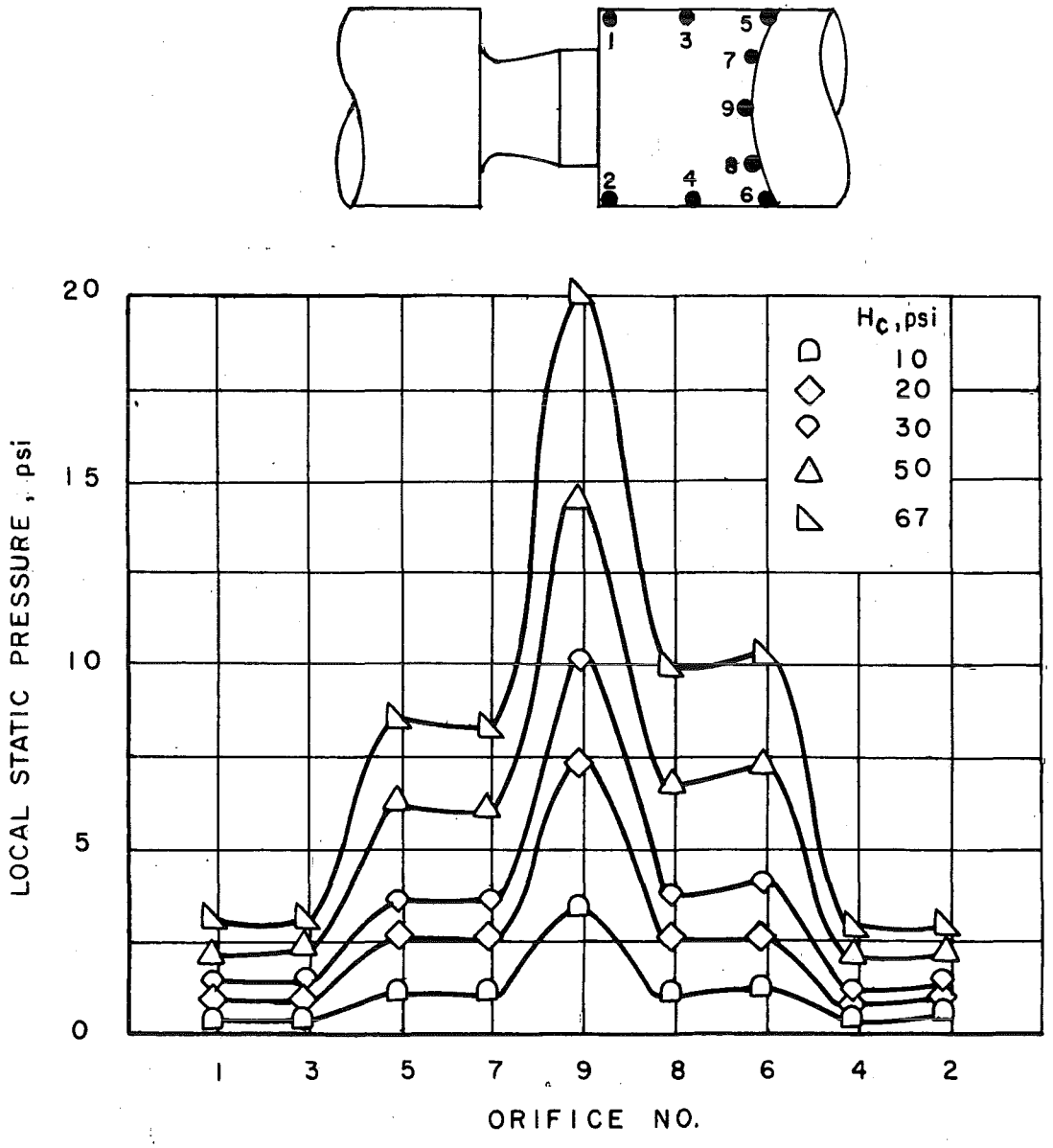

c. x/d = 1.04

Fig. 7 Concluded

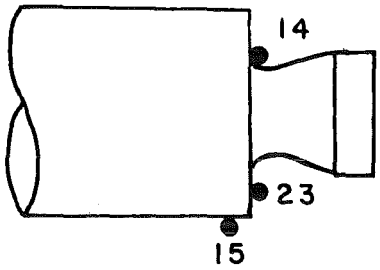

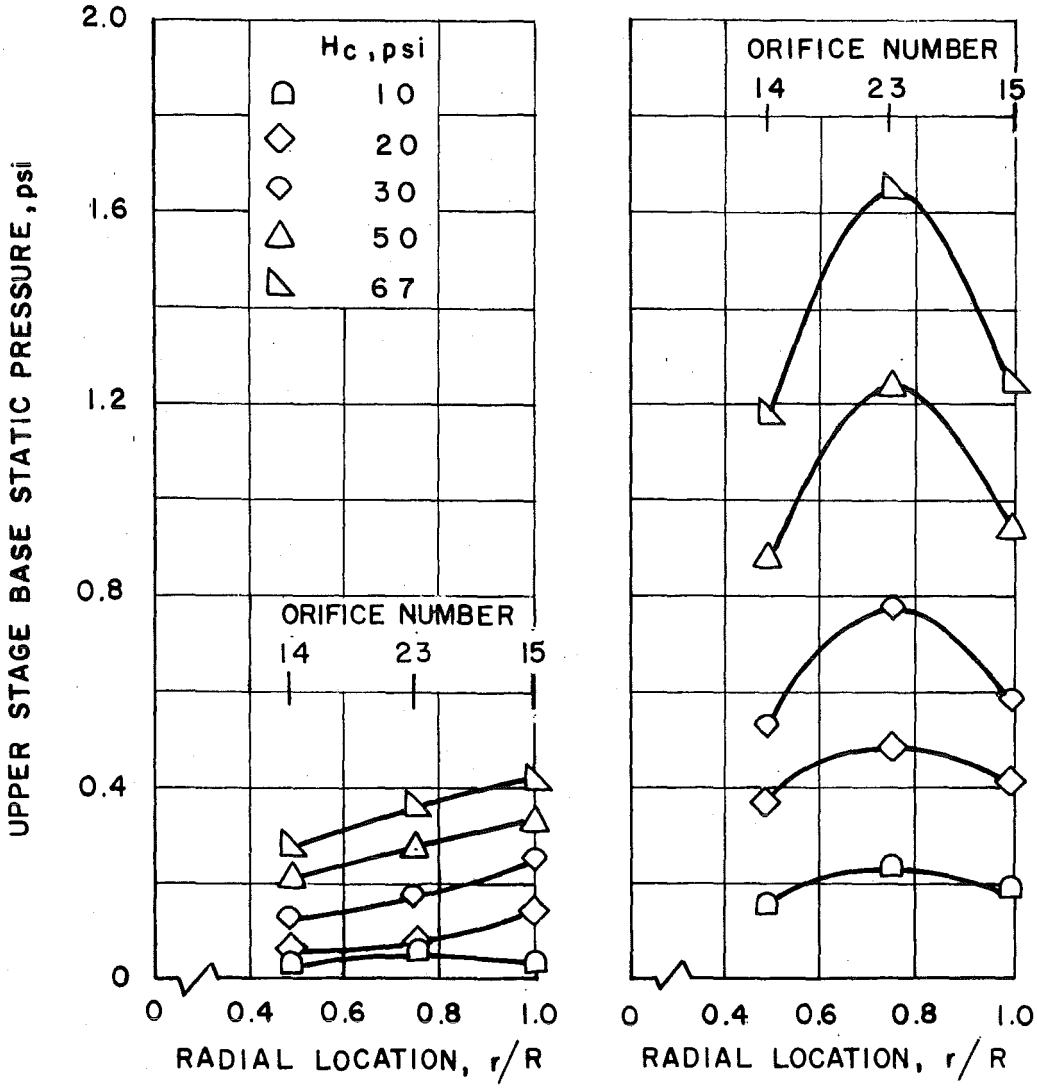

a. x/d = 1.54

b. x/d = 1.04

Fig. 8 Upper Stage Static Pressure Distribution

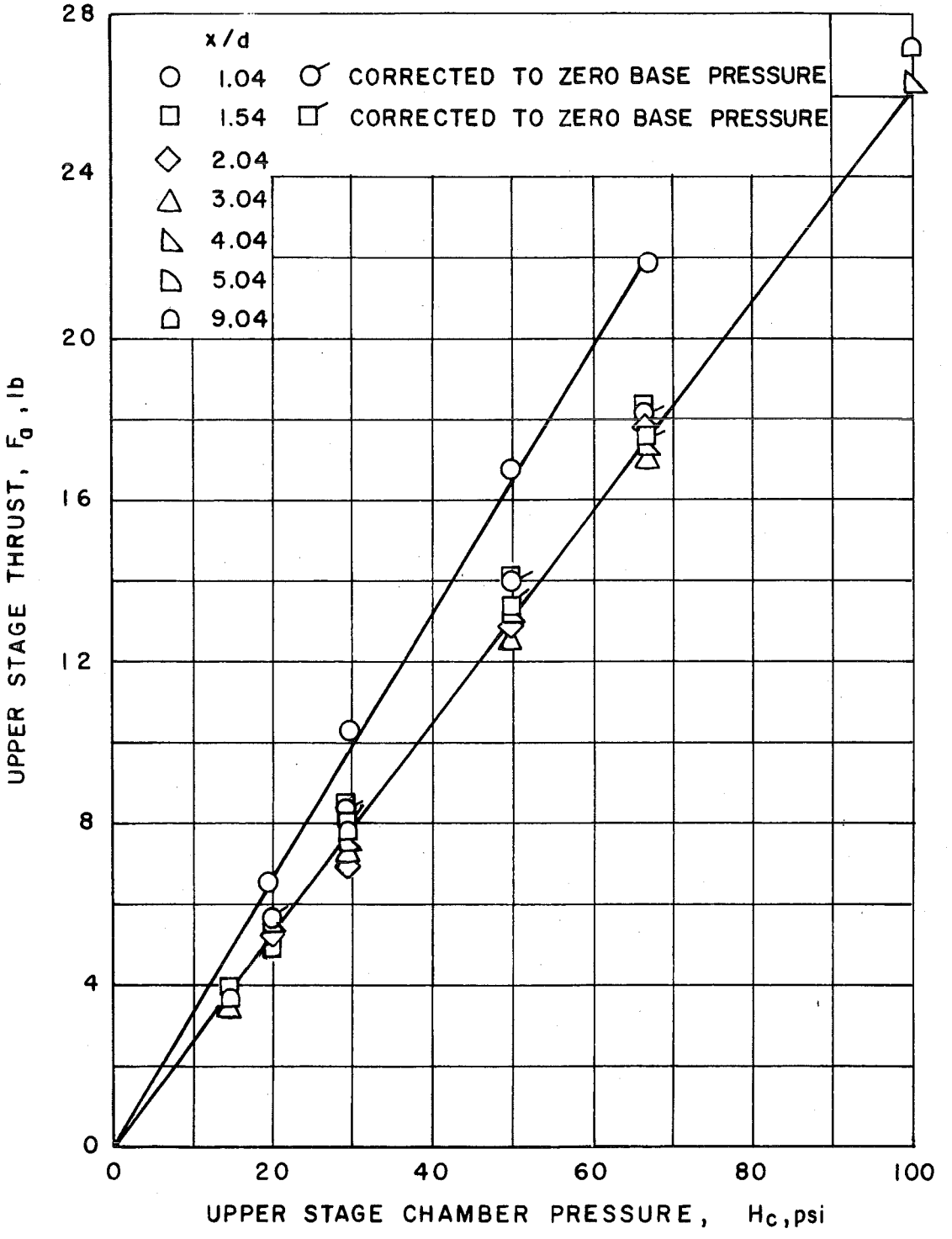

Fig. 9 Upper Stage Thrust

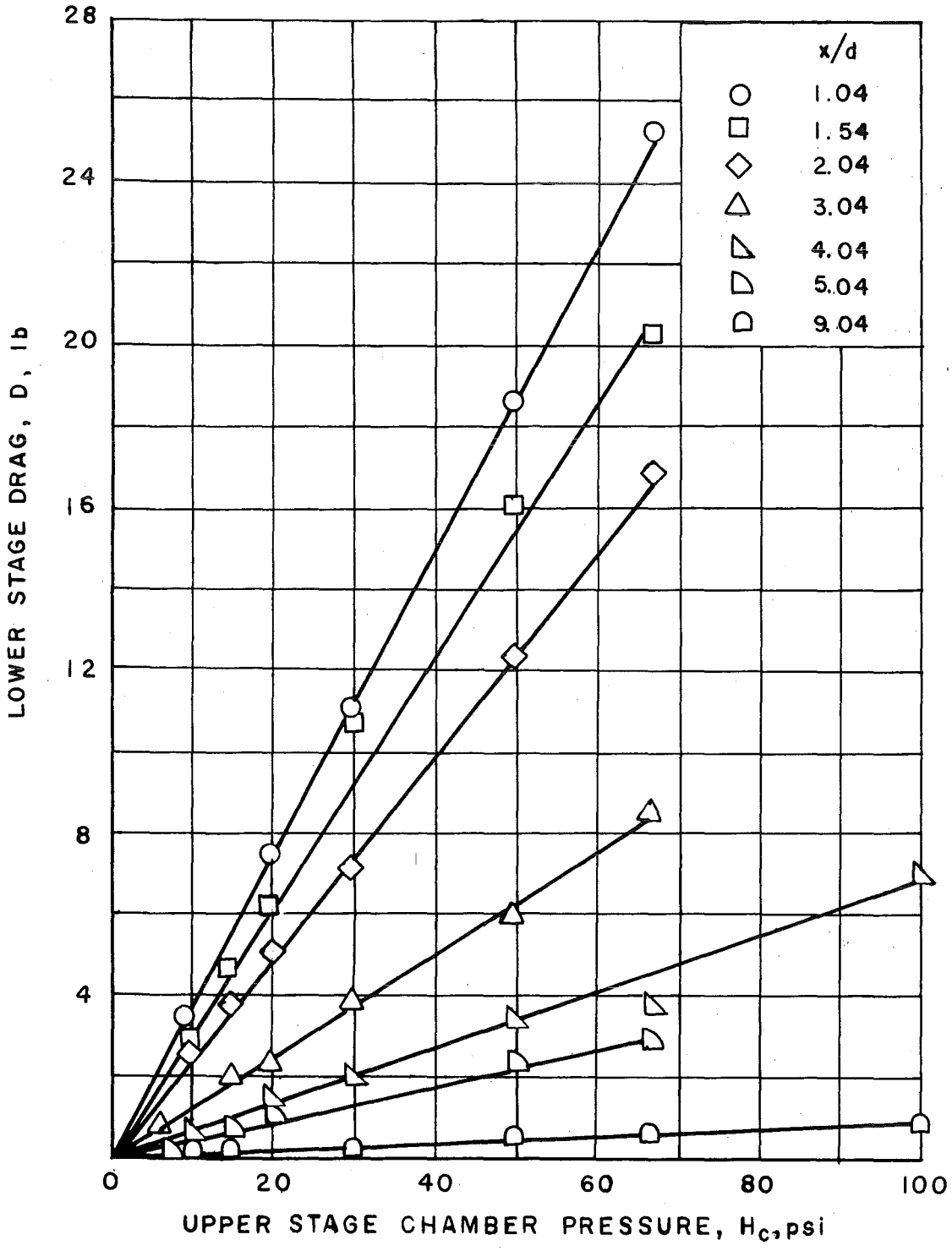

Fig. 10 Lower Stage Drag

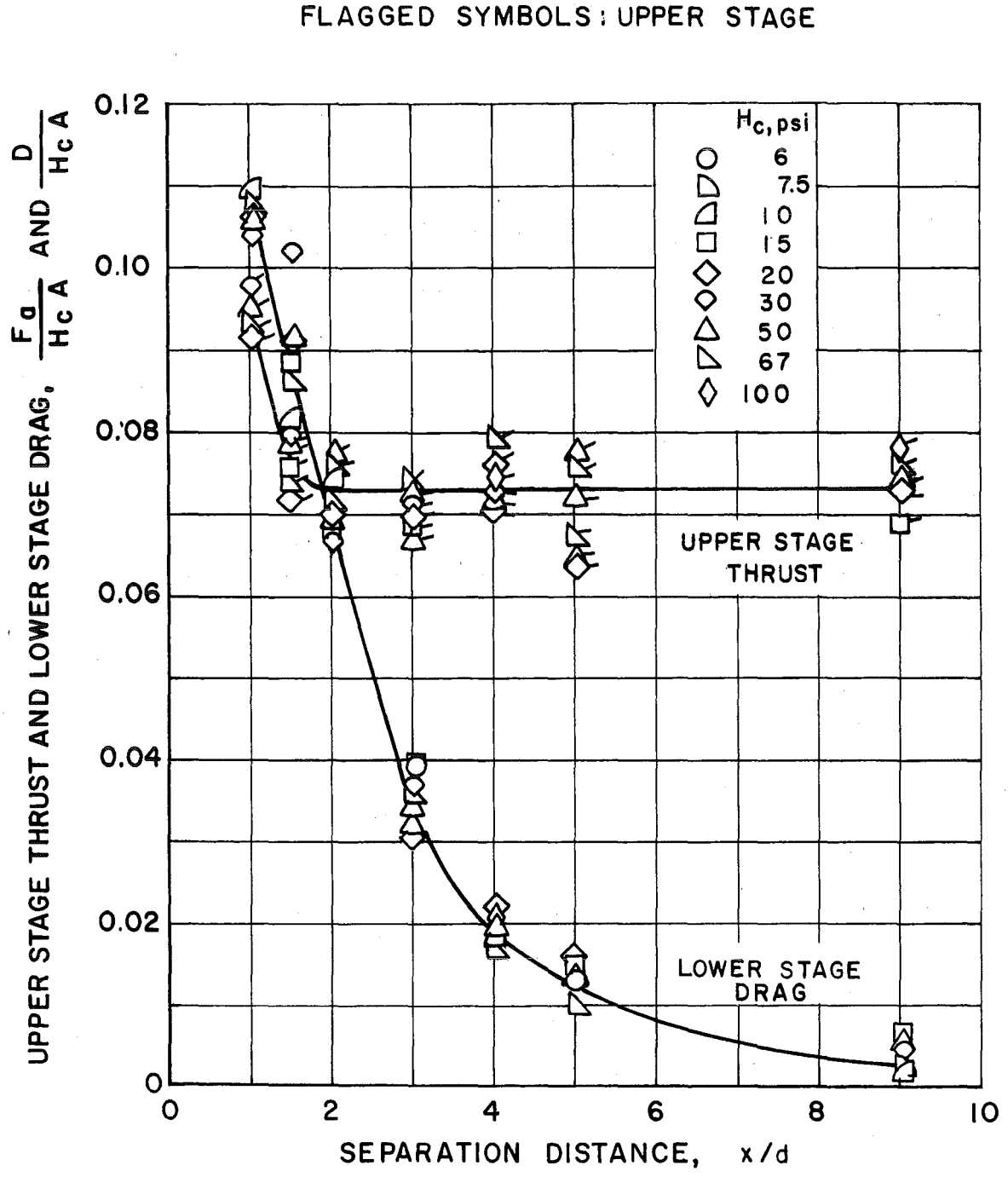

Fig. 11 Effect of Separation Distance on Axial Force